

Article

Air-to-Ground Path Loss Model at 3.6 GHz under Agricultural Scenarios Based on Measurements and Artificial Neural Networks

Hanpeng Li ¹, Kai Mao ¹, Xuchao Ye ¹, Taotao Zhang ², Qiuming Zhu ^{1,*} , Manxi Wang ², Yurao Ge ¹, Hangang Li ¹ and Farman Ali ¹

- ¹ The Key Laboratory of Dynamic Cognitive System of Electromagnetic Spectrum Space, College of Electronic and Information Engineering, Nanjing University of Aeronautics and Astronautics, Nanjing 211106, China; lihanpeng@nuaa.edu.cn (H.L.); maokai@nuaa.edu.cn (K.M.); yexuchao@nuaa.edu.cn (X.Y.); geyurao@nuaa.edu.cn (Y.G.); lihangang@nuaa.edu.cn (H.L.); farmanali@nuaa.edu.cn (F.A.)
- ² State Key Laboratory of Complex Electromagnetic Environment Effects on Electronics and Information System, Luoyang 471003, China; taotao_zhang123@126.com (T.Z.); manxi_wang@126.com (M.W.)
- * Correspondence: zhuqiuming@nuaa.edu.cn

Abstract: Unmanned aerial vehicles (UAVs) have found expanding utilization in smart agriculture. Path loss (PL) is of significant importance in the link budget of UAV-aided air-to-ground (A2G) communications. This paper proposes a machine-learning-based PL model for A2G communication in agricultural scenarios. On this basis, a double-weight neurons-based artificial neural network (DWN-ANN) is proposed, which can strike a fine equilibrium between the amount of measurement data and the accuracy of predictions by using ray tracing (RT) simulation data for pre-training and measurement data for optimization training. Moreover, an RT pre-correction module is introduced into the DWN-ANN to optimize the impact of varying farmland materials on the accuracy of RT simulation, thereby improving the accuracy of RT simulation data. Finally, channel measurement campaigns are carried out over a farmland area at 3.6 GHz, and the measurement data are used for the training and validation of the proposed DWN-ANN. The prediction results of the proposed PL model demonstrate a fine concordance with the measurement data and are better than the traditional empirical models.

Keywords: unmanned aerial vehicle (UAV); path loss (PL); agricultural scenario; artificial neural network (ANN); ray tracing (RT); channel measurement



Citation: Li, H.; Mao, K.; Ye, X.; Zhang, T.; Zhu, Q.; Wang, M.; Ge, Y.; Li, H.; Ali, F. Air-to-Ground Path Loss Model at 3.6 GHz under Agricultural Scenarios Based on Measurements and Artificial Neural Networks. *Drones* **2023**, *7*, 701. <https://doi.org/10.3390/drones7120701>

Academic Editor: Fei Liu

Received: 3 November 2023

Revised: 5 December 2023

Accepted: 7 December 2023

Published: 11 December 2023



Copyright: © 2023 by the authors. Licensee MDPI, Basel, Switzerland. This article is an open access article distributed under the terms and conditions of the Creative Commons Attribution (CC BY) license (<https://creativecommons.org/licenses/by/4.0/>).

1. Introduction

Thanks to their simple maneuverability, high agility, and cost-effectiveness, unmanned aerial vehicles (UAVs) are assuming a growing importance in agricultural applications including yield estimation, precision irrigation, and crop surveillance [1–4]. Path loss (PL) is a crucial large-scale parameter that has a substantial influence on the communication quality between ground stations and UAVs. Different from traditional terrestrial communications, the UAV-aided air-to-ground (A2G) channel demonstrates obvious three-dimensional (3D) characteristics [5,6], and the PL in agricultural scenarios also has some unique characteristics due to the influence of different farmland materials on the reflection or scattering process. Therefore, the modeling and accurate prediction of PL is of great significance in the construction and enhancement of UAV communication systems under agricultural scenarios.

Traditional PL predictions are primarily categorized into deterministic methods [7–13] and empirical methods [14–22]. For deterministic methods, PL is typically modeled through the ray tracing (RT) technique combined with environmental information. The authors in [7,8] utilized the RT technique to model the PL of urban scenarios, taking into account

the effects of transceiver locations and antenna heights, respectively. The authors in [9,10] predicted the PL under urban and forest scenarios, respectively, and both considered the additional impact of vegetation attenuation. For agricultural scenarios, the authors in [12] analyzed the channel characteristics of the narrowband internet of things under a typical rural scenario at 900 MHz by using the RT technique; they obtained the average PL between transceivers and derived the channel parameters including angular and delay spread. The authors in [13] developed a channel model for UAV-aided A2G radio frequency energy transfer based on the RT principle, which considered the influence of vegetation growth with time on PL in agricultural scenarios. Deterministic methods are generally considered to have a high accuracy. However, due to the complexity of ground materials caused by different types of crops in agricultural scenarios, there are inevitable differences between the reconstructed map materials and the real environment, which will affect the prediction accuracy. Moreover, deterministic methods normally come with high computational complexity.

Empirical methods usually model PL as a multi-factorial equation regarding some channel parameters including arrival angle, path delay, and so on. For example, the authors in [14,16] modeled the PL in scenarios involving rice and millet fields, respectively, as well as corn and soybean fields, and studied the effects of different crop growth stages on the PL. The authors in [17] measured the PL in a citrus plantation, and analyzed the measurement results based on the two-ray model, close-in (CI) free space reference distance PL model, and so on. For A2G scenarios, the authors in [20] investigated the effects of different transmission antenna heights on PL in rural scenarios at 26 GHz using a crane as a research platform, and analyzed the fitting performance of different empirical models, such as the CI and alpha-beta-gamma models. The authors in [21,22], respectively, studied channel parameters such as the received signal strength indicator of ZigBee and the WiFi link in farmland scenarios based on UAVs. Although empirical methods are relatively simple, they have poor scenario dependence and usually demand a substantial volume of measured data to calibrate the model. With the increase in scenario types, it is sometimes challenging to derive a general analytical equation.

Machine learning (ML) technology has attracted more and more interest in the field of channel parameter prediction due to its powerful data analysis ability [23–29]. For example, the authors in [24] evaluated the prediction accuracy of an artificial neural network (ANN) and various ML methods on PL by combining the measurement data in rural scenarios, and studied the impact of various neuron quantities and neural network (NN) layers on prediction performance. The authors in [25] utilized ML regressions to establish a PL model and investigated the impact of crop height and density at different growth stages of paddy and sugarcane on PL. The authors in [26] modeled the PL in different vegetation regions such as orange, cherry, pine, and walnut by using several ML methods such as recurrent NN. The authors in [28] applied different ensemble models to predict PL in rural scenarios for the first time, and designed the best ensemble technique. The authors in [29] predicted the PL in rural scenarios by using the k-nearest neighbor and random forest methods, and compared the predicted results with the conventional particle swarm optimization algorithm. ML methods typically demand a substantial volume of measured data during the training stage, which are rarely applied in rapidly moving UAV-aided A2G scenarios. In the case of insufficient measurement data, RT simulation data are usually employed as a substitute. Due to the complexity of ground materials and the limitation of map reconstruction accuracy in agricultural scenarios, there may be a certain disparity between RT simulation data and the actual results, which causes a decrease in the accuracy of the prediction results and greatly increases the limitations of NN applications. This study endeavors to fill this gap. The innovations and contributions are outlined as follows.

- A novel ML-based PL model with double-weight-neurons for UAV-aided A2G communications under agricultural scenarios is firstly proposed in this paper. The proposed model takes into account the main factors affecting PL, including signal propagation

distance, UAV height, and carrier frequency, and can accurately predict the PL of the line-of-sight (LoS) and non-LoS (NLoS) paths in the scenarios.

- A new ANN structure named double-weight neurons-based ANN (DWN-ANN) is designed for the PL model, which can solve the problem of large measurement data requirements in traditional ANNs and achieve accurate PL prediction through two-step training. Moreover, an RT pre-correction module is introduced to solve the problem of insufficient RT simulation accuracy caused by complex ground materials in agricultural scenarios.
- Channel measurement campaigns are carried out over a farmland area with different ground materials at 3.6 GHz. The measurement data are obtained for the training and validation of the proposed model. Moreover, the ground material parameters for RT simulations are modified. The prediction results demonstrate a fine concordance with the obtained data and achieve higher accuracy compared to the empirical models, which indicates that the proposed model can accurately predict the PL under agricultural scenarios.

The rest of the paper is structured as follows. Section 2 proposes the ML-based PL model under agricultural scenarios. In Section 3, the PL prediction scheme and the details of the DWN-ANN are introduced. Section 4 provides the channel measurement campaigns and a verification and comparison of the proposed PL model. Finally, the conclusions are summarized in Section 5.

2. Proposed ANN-Based PL Model

Numerous empirical and standardized models regarding PL prediction have been proposed, among which the third generation partnership project (3GPP) and CI models are particularly renowned. The CI model enhances PL prediction accuracy by introducing the PL exponent (PLE) based on the free-space PL (FSPL) model, which can be formulated as

$$PL_{CI}(f, d) = 10n \log_{10}(d/d_0) + PL_{FS}(f, d_0) + X_{\lambda}^{CI} \quad (1)$$

where d and f , respectively, represent the propagation distance and carrier frequency, d_0 represents the referenced distance which is typically set to 1 m, and n is the PLE of the CI model. X_{λ}^{CI} characterizes the shadow fading (SF), which follows a Gaussian distribution with a mean of zero and standard deviation of λ [30]. $PL_{FS}(f, d_0)$ represents the FSPL, which can be further expressed as

$$PL_{FS}(f, d_0) = 20 \log_{10}(f) + 20 \log_{10}(d_0) + 32.45 \quad (2)$$

The 3GPP model is considered to be a relatively authoritative PL model [31]. Taking the typical rural macro (RMa) scenario as an illustration, the 3GPP model under LoS and NLoS paths can be, respectively, expressed as

$$PL_{3GPP}^{LoS} = \begin{cases} PL_{3GPP}^1, 10m \leq d \leq d_P \\ PL_{3GPP}^2, d_P \leq d \leq 10km \end{cases} \quad (3)$$

$$PL_{3GPP}^{NLoS} = \max(PL_{3GPP}^{LoS}, PL_{3GPP}^3) \quad (4)$$

where PL_{3GPP}^1 , PL_{3GPP}^2 , and PL_{3GPP}^3 can be further expressed as

$$PL_{3GPP}^1 = \log_{10}(d) \times \min(10, 0.03h_B^{1.72}) - \min(14.77, 0.044h_B^{1.72}) + 20 \log_{10}(40\pi df/3) + 0.002d \times \log_{10}(h_B) \quad (5)$$

$$PL_{3GPP}^2 = PL_{3GPP}^1(d_P) + 40 \log_{10}(d/d_P) \quad (6)$$

$$\begin{aligned}
PL_{3GPP}^3 &= (\log_{10}(d) - 3) \times (43.42 - 3.1\log_{10}(h_{BS})) - 7.1\log_{10}(w_S) \\
&\quad - \log_{10}(h_{BS}) \times (24.37 - 3.7(h_B/h_{BS})^2) + 7.5\log_{10}(h_B) \\
&\quad - (3.2(\log_{10}(11.75h_{UT}))^2 - 4.97) + 20\log_{10}(f) + 161.04
\end{aligned} \tag{7}$$

where d_P represents the breakpoint distance, h_B represents the average height of buildings, w_S represents the average width of streets, and h_{UT} and h_{BS} , respectively, represent the antenna heights of the user terminal and base station.

Drawing inspiration from the principles of supervised learning in ML, we integrate traditional empirical models with ANN. By employing network architectures in place of explicit mathematical expressions, we aim to achieve more accurate predictions. Traditional NNs usually demand a substantial volume of measurement data during the training stage and it is difficult to acquire measurement data in scenarios like farmlands. Inspired by the NN's capability for second training, we designed a two-step training network named DWN-ANN. This network can conduct separate pre-training and optimized training by using RT simulation and measurement data to achieve a balance between prediction accuracy and the required amount of measurement data.

Farmland scenarios are typically characterized by open spaces and limited scatters. Therefore, the A2G channel in the farmland scenario can be modeled as consisting of one LoS path, one ground specular NLoS path, and some scattering NLoS paths. This paper aims to achieve the PL prediction of the LoS and NLoS paths separately. The proposed DWN-ANN-based PL model of LoS/NLoS cases can be formulated as

$$PL_{DWN-ANN}^{LoS/NLoS} = F_{DWN-ANN} \left(d^{LoS/NLoS}, h^{LoS/NLoS}, f^{LoS/NLoS} \middle| \mathbf{w}^{Total}, \mathbf{b}^{Total}, \sigma(\cdot) \right) \tag{8}$$

where $F_{DWN-ANN}(\cdot)$ is the transfer function of DWN-ANN determined by the network structure. $d^{LoS/NLoS}$, $h^{LoS/NLoS}$, and $f^{LoS/NLoS}$ are the input parameters of DWN-ANN, representing the propagation distance, UAV height, and carrier frequency, respectively. \mathbf{w}^{Total} and \mathbf{b}^{Total} are the total weight and bias matrices of DWN-ANN, respectively. $\sigma(\cdot)$ is the activation function. More details regarding the DWN-ANN structure will be elaborated in Section 3.

3. PL Prediction and DWN-ANN Design

3.1. Overview of PL Prediction Scheme

The overall PL prediction scheme is illustrated in Figure 1. In the first step, an A2G communication scenario is selected, and the measurement campaign is conducted in the chosen scenario to acquire measurement data, including the propagation distance, UAV height, carrier frequency, and the corresponding PL. Secondly, digital map reconstruction and RT simulation are carried out in the chosen scenario, and the RT pre-correction module is performed. Some of the measurement data are utilized to calibrate parameters such as the material conductivity for RT simulations. This calibration step aims to enhance the accuracy of the obtained RT simulation data significantly. Subsequently, the obtained dataset is split into the training and validation datasets, which are utilized for training the NN and assessing its performance, respectively. Finally, the DWN-ANN is constructed and the obtained RT simulation and measurement data are used for the pre-training and optimization training of the network, respectively. The trained DWN-ANN can accurately predict the PL by inputting a new propagation distance, UAV height, and carrier frequency.

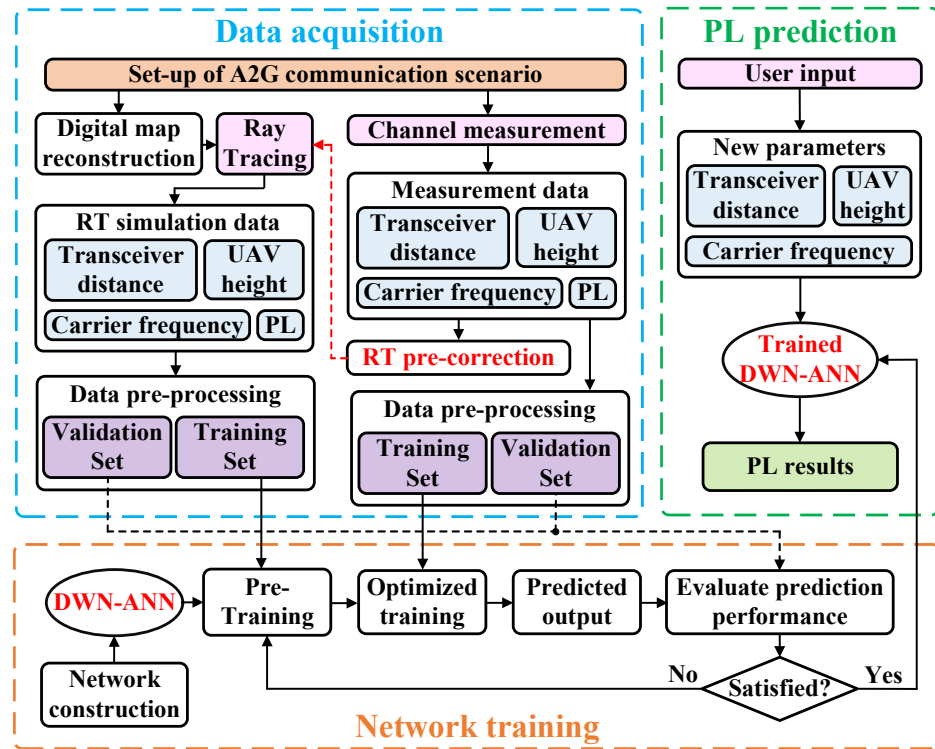


Figure 1. PL prediction scheme.

3.2. Network Structure

The proposed DWN-ANN consists primarily of a pre-training module (PTM) and an optimization training module (OTM), as illustrated in Figure 2. The PTM can utilize RT simulation data for preliminary training to learn the approximate relationship between the PL and other channel parameters. This enables the network to attain an initial stable state, reducing the required amount of measurement data and accelerating the network's convergence rate. After pre-training, the network parameters of PTM are assigned to the OTM. The OTM can utilize a modest quantity of measurement data for fine-tuning, leading to the further optimization of the network parameters and enhancement of prediction accuracy.

However, when conducting RT simulations in farmland scenarios, due to the limitation in the accuracy of reconstruction ground material, there might be significant disparities between the RT simulation data and the actual results. In such cases, relying solely on optimization with a small amount of measurement data might not be sufficient for error correction and achieving accurate PL prediction. Therefore, we also introduce an RT pre-correction module, utilizing the acquired measurement data to pre-correct parameters, such as the conductivity and relative dielectric constant of the ground material during RT simulations, so as to enhance the RT simulation accuracy.

During the pre-training phase, the network's input is the RT simulation data. In this phase, only the weight and bias matrices of PTM within the DWN-ANN are updated, while the weight and bias matrices of OTM remain constant. The predicted results of PTM can be formulated as

$$PL_{PTM}^{LoS/NLoS} = F_{DWN-ANN} \left(d_{RT-Train}^{LoS/NLoS}, h_{RT-Train}^{LoS/NLoS}, f_{RT-Train}^{LoS/NLoS} \mid \mathbf{w}^{PTM}, \mathbf{b}^{PTM}, \sigma(\cdot) \right) \quad (9)$$

where $d_{RT-Train}^{LoS/NLoS}$, $h_{RT-Train}^{LoS/NLoS}$, and $f_{RT-Train}^{LoS/NLoS}$ are the training set of propagation distance, UAV height, and carrier frequency obtained through the RT method, respectively. \mathbf{w}^{PTM} and \mathbf{b}^{PTM} are the weight and bias matrices of PTM, respectively.

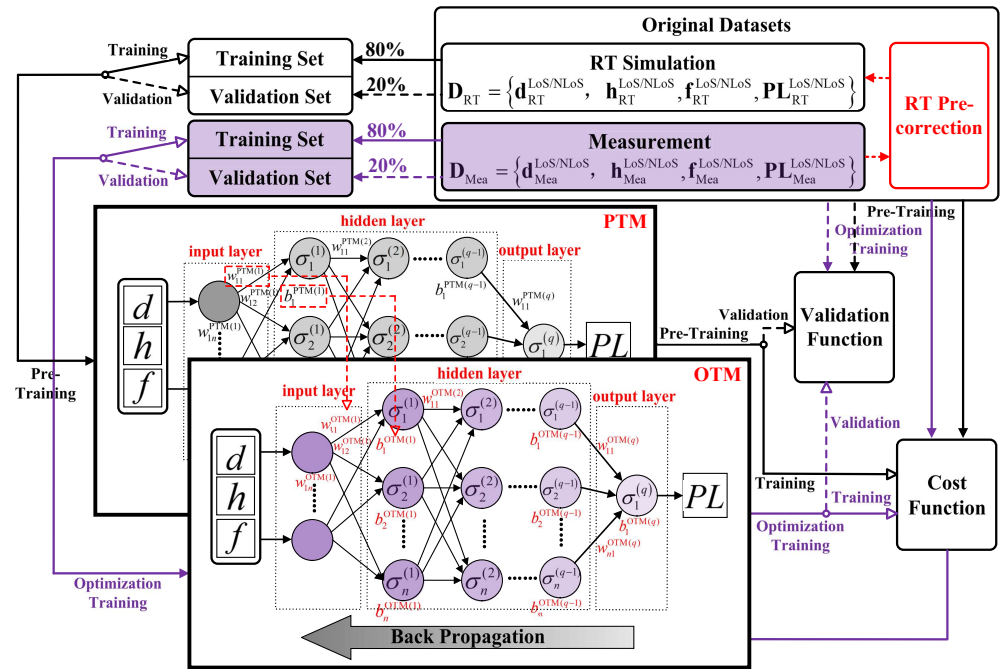


Figure 2. Network structure of proposed DWN-ANN.

After pre-training, the network proceeds to the optimization training phase, with the network’s input changing to the training set of measurement data. At this point, the weight and bias matrices of PTM retain the pre-trained values and are assigned to the OTM. Subsequently, the network performs optimization training using the measurement data, fine-tuning the weight and bias matrices of OTM. The predicted results of OTM can be formulated as

$$PL_{OTM}^{LoS/NLoS} = F_{DWN-ANN} \left(d_{Mea-Train}^{LoS/NLoS}, h_{Mea-Train}^{LoS/NLoS}, f_{Mea-Train}^{LoS/NLoS}, \mathbf{w}^{PTM}, \mathbf{b}^{PTM} \mid \mathbf{w}^{OTM}, \mathbf{b}^{OTM}, \sigma(\cdot) \right) \quad (10)$$

where $d_{Mea-Train}^{LoS/NLoS}$, $h_{Mea-Train}^{LoS/NLoS}$, and $f_{Mea-Train}^{LoS/NLoS}$ are the training set of propagation distance, UAV height, and carrier frequency obtained through channel measurement, respectively. \mathbf{w}^{OTM} and \mathbf{b}^{OTM} are the weight and bias matrices of OTM, respectively.

Taking the classic three-layer NN structure, including an input layer, a single hidden layer comprising N neurons, and an output layer as an illustration, the final prediction results of the DWN-ANN-based PL prediction algorithm can be formulated as

$$PL_{DWN-ANN}^{LoS/NLoS} = F_{DWN-ANN} \left(d_{Train}^{LoS/NLoS}, h_{Train}^{LoS/NLoS}, f_{Train}^{LoS/NLoS} \mid \mathbf{w}^{Total}, \mathbf{b}^{Total}, \sigma(\cdot) \right) \\ = \sigma_O \left(\sum_{n=1}^N \left(w_{n1}^{PTM(2)} w_{n1}^{OTM(2)} \sigma_H \left(w_{1n}^{PTM(1)} w_{1n}^{OTM(1)} d_{Train}^{LoS/NLoS} + w_{2n}^{PTM(1)} w_{2n}^{OTM(1)} h_{Train}^{LoS/NLoS} + \right) \right) + b_1^{PTM(2)} b_1^{OTM(2)} \right) \quad (11)$$

where $w_{pq}^{PTM(1/2)} \in \mathbf{w}^{PTM}$ and $b_q^{PTM(1/2)} \in \mathbf{b}^{PTM}$ represent the connection weights and biases of the hidden/output layer neurons in the PTM, respectively. $w_{pq}^{OTM(1/2)} \in \mathbf{w}^{OTM}$ and $b_q^{OTM(1/2)} \in \mathbf{b}^{OTM}$ represent the connection weights and biases of the hidden/output layer neurons in the OTM, respectively. $\sigma_{H/O}(\cdot) \in \sigma(\cdot)$ represents the activation functions of the hidden/output layer. \mathbf{w}^{Total} and \mathbf{b}^{Total} can be calculated as the product of the corresponding elements in \mathbf{w}^{PTM} and \mathbf{w}^{OTM} , as well as the product of the corresponding elements in \mathbf{b}^{PTM} and \mathbf{b}^{OTM} , respectively.

N , which represents the neuron quantity of the hidden layer, significantly impacts the prediction performance and can be calculated as

$$N = \sqrt{N_I + N_O} + a_{\text{Neuron}} \quad (12)$$

where N_I and N_O are the neuron quantity of the input and output layer, respectively. a_{Neuron} is typically a constant with a value within the range of $[1, 10]$.

The introduction of activation functions enables the NN to exhibit non-linearity. The hidden layer applies the leaky rectified linear unit (LeakyReLU) function [32], which can solve the “neuron death” problem in the traditional rectified linear unit (ReLU) function and has a faster convergence rate, as shown in (13). The output layer applies the Purelin function, as illustrated in (14).

$$\sigma_{\text{LeakyReLU}}(x) = \max(x, 0) + a_{\text{LeakyReLU}} \min(x, 0) \quad (13)$$

$$\sigma_{\text{Purelin}}(x) = x \quad (14)$$

where $a_{\text{LeakyReLU}}$ is a non-zero slope, typically set to 0.01.

The essence of network training is to minimize the loss function value as much as possible by continuously iterating and adjusting the network parameters. Therefore, the design of the loss function directly impacts the training performance. The introduction of L2 regularization in loss functions makes the network more inclined to use smaller and more dispersed weight vectors, ensuring that all input features are considered during training, which can enhance the model’s generalization ability and reduce the risk of overfitting. The loss function of PTM and OTM based on the mean square error and adding L2 regularization can be, respectively, expressed as

$$L_{\text{PTM}}^{\text{LoS/NLoS}} = \frac{1}{I} \sum_{i=1}^I \left(PL_{\text{PTM}}^{\text{LoS/NLoS}} \left(d_{\text{RT-Train},i}^{\text{LoS/NLoS}}, h_{\text{RT-Train},i}^{\text{LoS/NLoS}}, f_{\text{RT-Train},i}^{\text{LoS/NLoS}} \right) - PL_{\text{RT-Train},i}^{\text{LoS/NLoS}} \right)^2 + \frac{1}{2} \mu \sum_{k=1}^K \left\| \mathbf{w}^{\text{PTM}(k)} \right\|^2 \quad (15)$$

$$L_{\text{OTM}}^{\text{LoS/NLoS}} = \frac{1}{I} \sum_{i=1}^I \left(PL_{\text{OTM}}^{\text{LoS/NLoS}} \left(d_{\text{Mea-Train},i}^{\text{LoS/NLoS}}, h_{\text{Mea-Train},i}^{\text{LoS/NLoS}}, f_{\text{Mea-Train},i}^{\text{LoS/NLoS}} \right) - PL_{\text{Mea-Train},i}^{\text{LoS/NLoS}} \right)^2 + \frac{1}{2} \mu \sum_{k=1}^K \left\| \mathbf{w}^{\text{OTM}(k)} \right\|^2 \quad (16)$$

where I represents the quantity of samples within the training dataset, K represents the quantity of layers within the NN, and μ represents the regularization factor of L2 regularization.

The update of network weights and biases during each iteration can be, respectively, expressed as

$$w_{pq}^{\text{PTM/OTM}(k)} = w_{pq}^{\text{PTM/OTM}(k)} - \eta \frac{\partial L_{\text{PTM/OTM}}^{\text{LoS/NLoS}}}{\partial w_{pq}^{\text{PTM/OTM}(k)}} + \omega \Delta w_{pq}^{\text{PTM/OTM}(k)} \quad (17)$$

$$b_q^{\text{PTM/OTM}(k)} = b_q^{\text{PTM/OTM}(k)} - \eta \frac{\partial L_{\text{PTM/OTM}}^{\text{LoS/NLoS}}}{\partial b_q^{\text{PTM/OTM}(k)}} + \omega \Delta b_q^{\text{PTM/OTM}(k)} \quad (18)$$

where $\partial(\cdot)$ represents the partial derivative, η represents the learning rate of the NN, and ω represents the momentum factor, which can prevent the network parameters from getting stuck in local minima during updates. After continuous iterative training, the trained DWN-DNN can achieve an accurate prediction of the PL.

3.3. RT Data Pre-Correction

Due to the complex composition of farmland types, which includes a mixture of crops, earth, and water, it is challenging to accurately reconstruct them for RT simulations. Consequently, the obtained RT simulation data often exhibit significant discrepancies with the actual results, leading to the lower training accuracy of the PTM in DWN-ANN. In light of this, we designed the RT pre-correction module, which utilizes the measurement data to invert the real conductivity and relative dielectric constant of the ground material during RT simulation, so as to improve the accuracy of the obtained RT simulation data.

The measured farmland can be further divided into different sub-scenarios, and a preliminary 3D map reconstruction of the farmland is carried out, where the conductivity and relative dielectric constant of the ground material are initially set to default values of the grassland. Then, RT simulations are performed on the farmland scenario to calculate the NLoS path reflection points corresponding to different UAV locations. Furthermore, by combining the actual GPS coordinates of the UAV with the calculated reflection point positions, the measurement data generated by reflections on the ground in different sub-scenarios are divided into different groups. Finally, the measurement data from different sub-scenarios are compared with the corresponding RT data, and the ground material parameters for each sub-scenario are continuously adjusted until the generated RT data match the measurement data.

After RT pre-correction, more accurate RT simulation data can be obtained in the farmland scenario, improving the accuracy of the PTM in DWN-ANN and further reducing the amount of measurement data required by the OTM.

4. Validation and Comparison

4.1. Channel Measurement Campaigns

Most of the existing A2G channel measurement campaigns are predominantly focused on urban scenarios, with relatively fewer studies conducted in rural farmland scenarios. Furthermore, only a few of them consider different UAV heights. In this study, we conduct measurement campaigns of different UAV heights in a farmland scenario.

The developed A2G channel sounder is illustrated in Figure 3, including a UAV-aided transmitter (TX) and a receiver (RX) fixed on the ground, as shown in Figure 3a and Figure 3b, respectively. The TX comprises a hexacopter UAV, an omnidirectional antenna, a global positioning system (GPS) antenna, and a software-defined radio (SDR) signal transmitting platform comprising a radio frequency (RF) module, a high-power amplifier (HPA), and a lithium battery. The sounding signal is sent through the RF module, HPA, and omnidirectional antenna. The independent lithium battery is used for the power supply for both the HPA and RF modules. The RX consists of an omnidirectional antenna, a GPS module, an uninterruptible power supply, and an SDR signal processing platform comprising an RF module and a baseband processing module. The received signal is captured by the omnidirectional antenna, and then sent into the baseband processing module through the RF module for data processing. Finally, the measurement data are stored in the disk. Data transmission between the SDR and disk is realized via the PCIE bus. The comprehensive specifications of the channel sounder are introduced in Table 1, and more details about the channel sounder can be found in [33].

Table 1. Hardware parameters of the A2G channel sounder.

System Parameters	Values
Supported frequency band	100–6000 MHz
Bandwidth	100 MHz
Transmit power	32 dBm
HPA gain	42 dB
Antenna type	Omnidirectional Antenna
Antenna gain	2.5 dBi
Measurement sequence	Single-tone signal/Zadoff-Chu (ZC) sequence

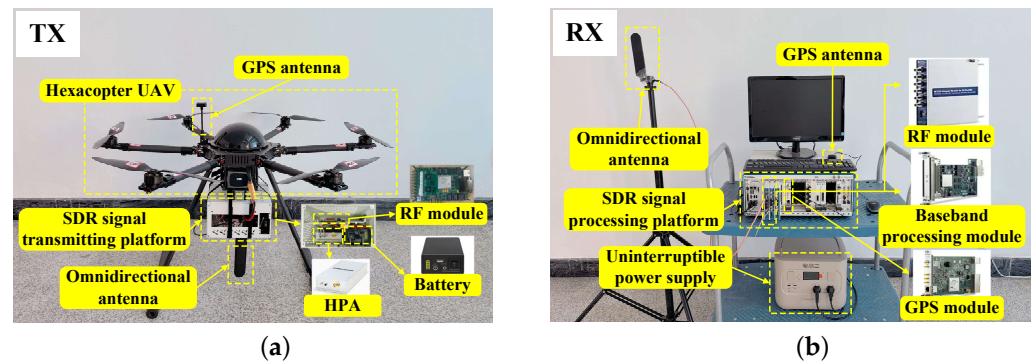


Figure 3. Overview of the (a) TX and (b) RX of the A2G channel sounder.

The channel measurement was conducted on a farmland at 3.6 GHz, and the ZC sequence is used in the channel sounder. The farmland area was approximately 150 m by 120 m, with sparse roads and low-rise buildings scattered around, resulting in an overall open environment. The RX was positioned at the edge of the farmland with the antenna at a height 2.5 m above the ground. The GPS coordinates for the fixed RX point were 118.57402 E 33.09518 N. Since the UAV normally flies at low altitudes for operations like yield estimation, precise irrigation, and crop monitoring in agricultural scenarios, we selected the UAV height range of 10 m to 30 m for the channel measurement campaigns. The UAV, equipped with the TX, took off from one side of the farmland and flew in a straight line with a 5 m height interval at different heights ranging from 10 m to 30 m and a flight distance of 100 m for each height, as shown in Figure 4. The GPS coordinates for the starting point of the horizontal movement of TX were 118.5736 E 33.09546 N. The receiver only started recording channel data when the UAV flew along the solid yellow line in the figure and stopped recording when it flew along the dashed yellow line. The PL data corresponding to different distances and UAV altitudes were obtained.

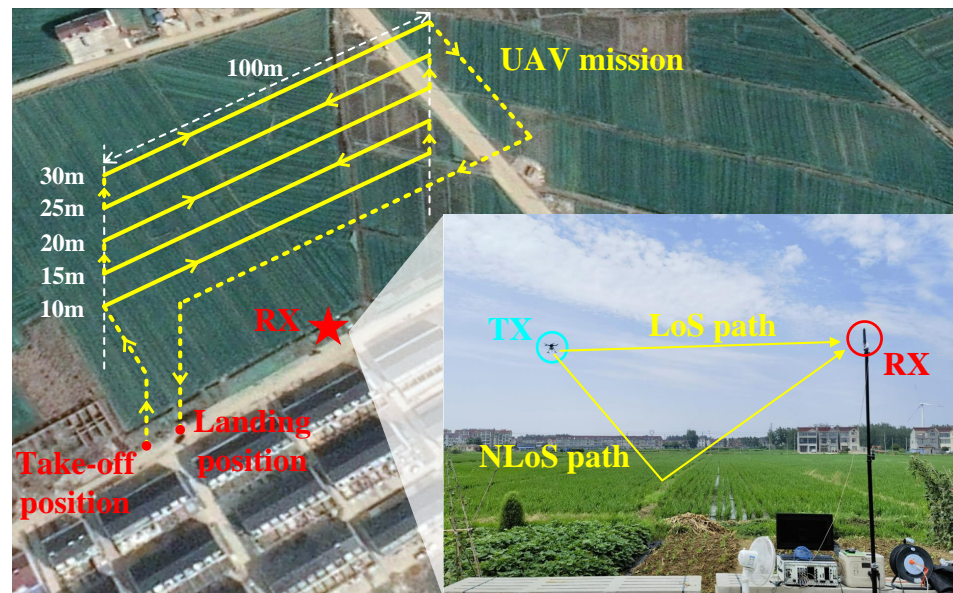


Figure 4. Channel measurement campaigns in the farmland scenario.

4.2. Data Pre-Processing

We further divided the measured farmland into four sub-scenarios: crops with dry earth, crops with wet earth, paddy fields, and dense crops (without exposed earth), as shown in Figure 5. After the channel measurement, we corrected the electromagnetic

parameters of the ground materials for RT simulations based on some of the measurement data. The modified electromagnetic parameters of different materials are shown in Table 2.

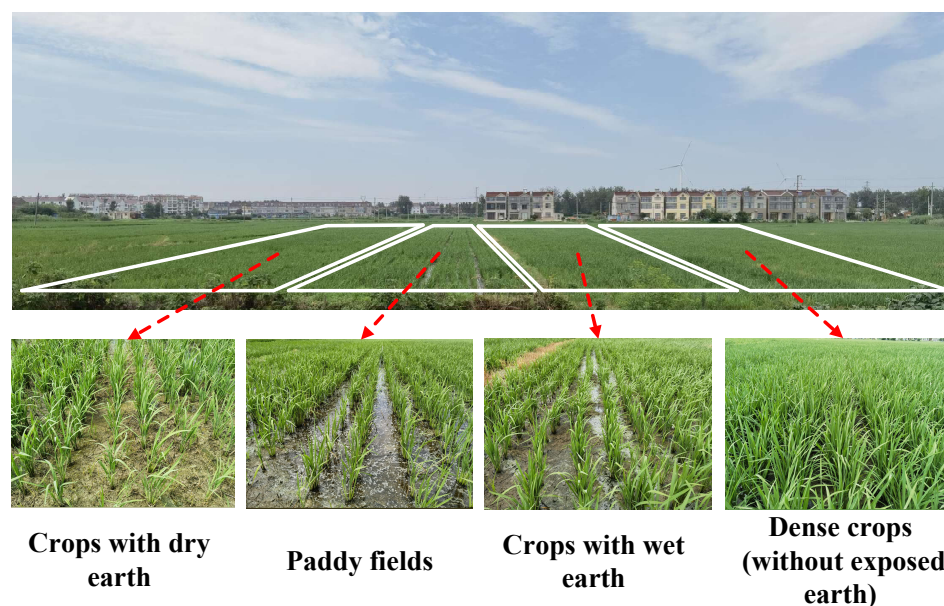


Figure 5. Four types of sub-scenarios in the farmland area.

Table 2. Modified electromagnetic parameters of four ground materials.

Ground Material	Relative Dielectric Constant	Conductivity (S/m)
Crops with dry earth	2.12	0.001
Crops with wet earth	2.2	0.018
Paddy fields	1.85	0.18
Dense crops (without exposed earth)	2.1	0.15

4.3. Prediction Results Analysis

In total, we obtained 10,000 RT simulation data and 5065 measurement data, then divided the obtained RT data and measurement data, respectively, into the training dataset and validation dataset in proportions of 80% and 20%. The RT training dataset was utilized for the initial training of the PTM, followed by the measurement training dataset being utilized for the optimization training of the OTM. It should be mentioned that, in order to verify the property that our proposed model can decrease the usage of measurement data while ensuring the prediction accuracy, only 30% of the measurement training dataset was utilized to further optimize the OTM. For the network structure, the input parameters of both PTM and OTM were the propagation distance, UAV height, and carrier frequency, and the output parameter was the PL. Therefore, the number of nodes in the input and output layers were set to 3 and 1, respectively. The number of hidden layers was set to 2, with each layer comprising 10 nodes. The PTM and the OTM had the same network structure in order to ensure the successful transmission of network parameters. The Adam optimizer was employed in the NN to ensure the correct update of the loss function parameters with a suitable magnitude, and the learning rate was configured as 0.001. After training, the prediction results were compared with the remaining 20% validation set.

For the LoS case, the prediction results of the proposed model, 3GPP, and CI model at UAV heights of 10 m and 20 m are shown in Figure 6. We can see that the PLEs of the CI model were fitted to 2.15 at a UAV height of 10 m and 2.26 at a height of 20 m, respectively. The standard deviations of SF were 3.031 dB and 3.279 dB, respectively. The 3GPP model was obtained through the formula of the LoS case under RMA in [31], where the average

height of buildings was set to 5 m. For comparison purposes, the RT validation dataset and measurement validation dataset are drawn in the figure as well.

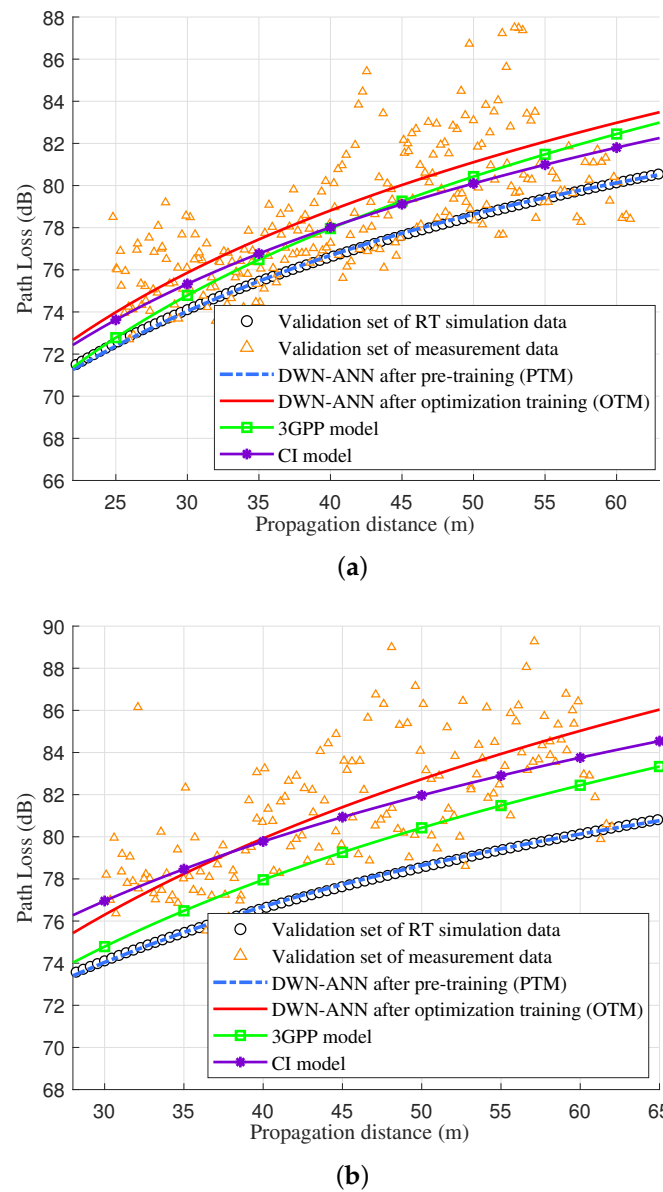


Figure 6. DWN-ANN, RT validation dataset, measurement validation dataset, 3GPP, and CI model of LoS case at UAV heights of (a) 10 m and (b) 20 m.

As shown in Figure 6, since the PL of the LoS path was not affected by the scatterer materials, the obtained RT simulation data relatively align with the measurement data. The measured PLs were slightly influenced by the elevation angles of the propagation paths because the actual antenna pattern was not perfectly isotropic. The predicted PL of DWN-ANN after pre-training and optimization training were, respectively, consistent with the RT validation dataset and measurement validation dataset, which demonstrates the accuracy of the proposed model. Moreover, the predicted values of our proposed model were consistent with the 3GPP model and closer to the measurement data than the CI model, which verifies that the proposed model conforms to the 3GPP standard and is superior to the traditional empirical model, allowing for the accurate prediction of the PL of the LoS path in the farmland scenario.

For the NLoS case, the prediction results of the proposed model, 3GPP, and CI model at UAV heights of 15 m and 30 m are given in Figure 7. Here, default grassland ground

material parameters were utilized to acquire RT simulation data without RT pre-correction. The 3GPP model was obtained through the formula of NLoS case under RMa in [31], where the average height of buildings was set to 5 m, the average width of streets was set to 4 m, the antenna height of the user terminal was set to 2.5 m, and the antenna height of the base station was set according to the different UAV heights. The PLEs of the CI model at UAV heights of 15 m and 30 m were, respectively, fitted to 2.79 and 2.88, which are slightly smaller than the PLE in urban scenarios. The standard deviations of SF were 3.652 dB and 4.112 dB, respectively.

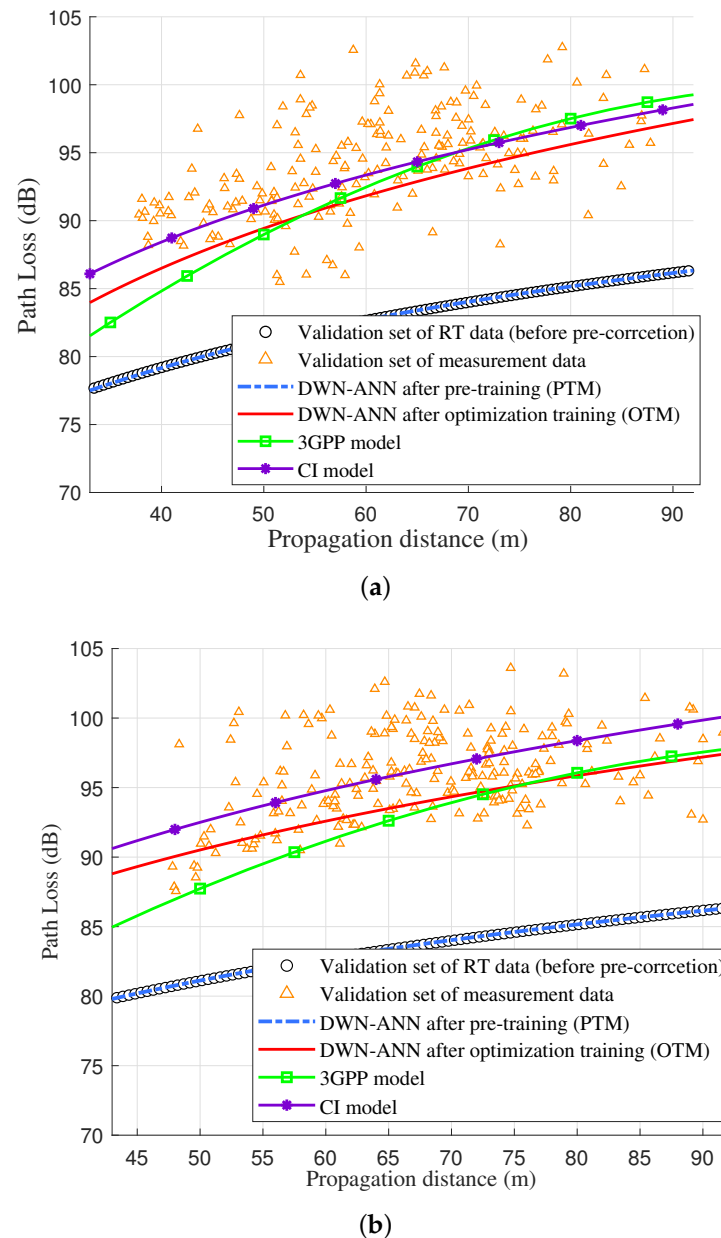
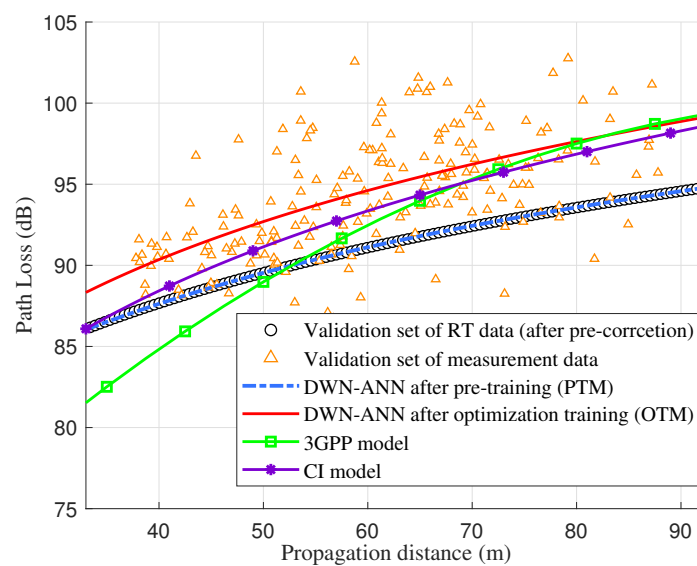


Figure 7. DWN-ANN (without RT pre-correction), RT validation dataset, measurement validation dataset, 3GPP, and CI model of NLoS case at UAV heights of (a) 15 m and (b) 30 m.

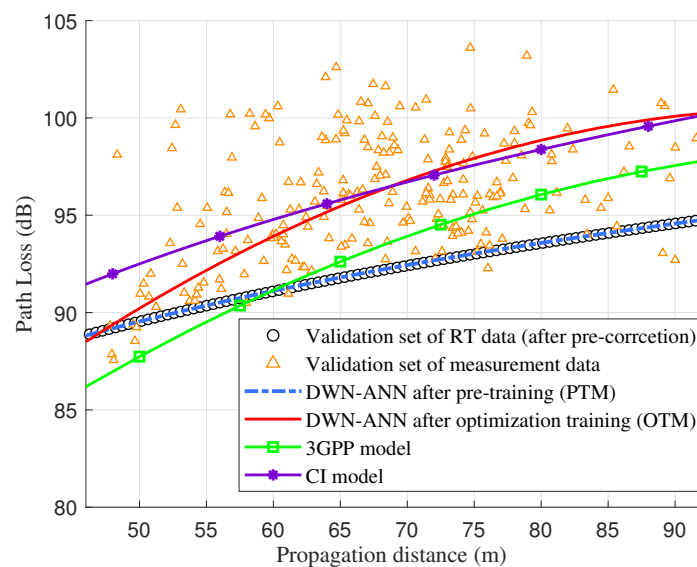
Due to the complexity of the ground materials and the significant influence of ground materials on the ground reflection path, without RT pre-correction, there was a relatively significant difference between the obtained RT simulation data and the measurement data. It was found that the prediction results of DWN-ANN after pre-training still matched the RT validation dataset, but the corresponding results after optimization training were slightly lower than the measurement data, which demonstrates a decreased prediction

accuracy in comparison to the LoS case. However, the predicted PL was still close to the 3GPP and CI model, indicating the validity of the proposed model. Even when using default RT material parameters and with limited measurement data, the DWN-ANN can still improve prediction accuracy through joint training with RT and measurement data, achieving similar prediction results to traditional models.

After RT pre-correction, the corresponding prediction values are illustrated in Figure 8. As depicted in the figure, after correcting ground material parameters of the farmland using measurement data, the obtained RT simulation data of NLoS path were in better agreement with the measurement data. The predicted PL of DWN-ANN after pre-training and optimization training, respectively, aligned with the RT validation dataset and measurement validation dataset, and were closer to the measurement data than 3GPP and CI model, which indicates the superiority of our proposed model in the NLoS case, which can accurately predict the PL of the NLoS path in the farmland scenario. Furthermore, it also proves the necessity of the RT pre-correction module in scenarios with complex materials.



(a)



(b)

Figure 8. DWN-ANN (with RT pre-correction), RT validation dataset, measurement validation dataset, 3GPP, and CI model of NLoS case at UAV heights of (a) 15 m and (b) 30 m.

In order to intuitively demonstrate the prediction accuracy of different models, the root mean square error (RMSE) between the measurement data and the CI model, 3GPP model, and the proposed DWN-ANN model is shown in Table 3. According to the above analysis, it can be concluded that the ground materials of farmland scenarios significantly impact the RT simulation accuracy. Our proposed model can achieve similar prediction accuracy to traditional CI and 3GPP models when using default ground materials in RT simulation. After the pre-correction of the ground material parameters, the prediction values are consistent with the measurement data and superior to traditional models. In summary, the proposed model can achieve a favorable equilibrium between prediction accuracy and the required amount of measurement data through joint training with RT and measurement data. Moreover, it can enhance prediction accuracy via RT pre-correction, achieving accurate PL prediction under LoS and NLoS paths in farmland scenarios. The proposed model solves the issue of PL prediction in the case of insufficient measurement data and inaccurate RT simulation in the farmland scenario.

Table 3. The RMSE of CI model, 3GPP model, and the proposed DWN-ANN model.

	Figure 6a	Figure 6b	Figure 7a	Figure 7b	Figure 8a	Figure 8b
CI model	2.1912	2.3071	3.4089	2.8562	3.4089	2.8562
3GPP model	2.2732	3.1757	4.1951	4.1922	4.1951	4.1922
DWN-ANN	2.1727	2.2877	4.0231	3.5267	3.2425	2.7330

5. Conclusions

This paper has proposed an ML-based PL model under agricultural scenarios. A new network structure named DWN-ANN has been developed to predict the PL of the LoS and NLoS paths, which can be pre-trained and further optimized by using RT simulation and measurement data, respectively. Furthermore, an RT pre-correction module has been introduced to optimize the RT simulation accuracy, and modified material electromagnetic parameters have been given. To thoroughly analyze and appraise the proposed model, extensive channel measurement campaigns have been conducted over farmland areas at 3.6 GHz. Through a comparison with the measurement data, our proposed model has been proven to be more accurate than traditional models. This suggests that our model is better suited for UAV-aided A2G communications in agricultural scenarios. In the future, it is envisaged that measurement campaigns will be conducted on diverse farmland areas with the aim of substantiating the proposed model's universality.

Author Contributions: Conceptualization, H.L. (Hanpeng Li) and Q.Z.; funding acquisition, Q.Z. and F.A.; investigation, K.M. and X.Y.; methodology, H.L. (Hanpeng Li); software, H.L. (Hanpeng Li) and X.Y.; data acquisition, Y.G. and H.L. (Hangang Li); supervision, Q.Z. and F.A.; validation, T.Z. and M.W.; writing—original draft, H.L. (Hanpeng Li) and K.M. All authors have read and agreed to the published version of the manuscript.

Funding: This work was supported, in part, by the National Natural Science Foundation of China under Grant No. 62271250; in part by the Natural Science Foundation of Jiangsu Province, No. BK20211182; in part by the Key Technologies R&D Program of Jiangsu (Prospective and Key Technologies for Industry) under Grants BE2022067, BE2022067-1, and BE2022067-3; and in part by the open research fund of the National Mobile Communications Research Laboratory, Southeast University, No. 2022D04.

Data Availability Statement: The datasets collected and generated in this study are available upon request to the corresponding author.

Conflicts of Interest: The authors declare no conflict of interest.

References

1. Shakhathreh, H.; Sawalmeh, A.H.; Al-Fuqaha, A.; Dou, Z.; Almaita, E.; Khalil, I.; Othman, N.S.; Khreishah, A.; Guizani, M. Unmanned aerial vehicles (UAVs): A survey on civil applications and key research challenges. *IEEE Access* **2019**, *7*, 48572–48634. [\[CrossRef\]](#)
2. Galán-Jiménez, J.; Vegas, A.G.; Berrocal, J. Energy-efficient deployment of IoT applications in remote rural areas using UAV networks. In Proceedings of the WMNC'22, Sousse, Tunisia, 17–19 October 2022; pp. 70–74. [\[CrossRef\]](#)
3. Shi, M.; Yang, K.; Niyato, D.; Yuan, H.; Zhou, H.; Xu, Z. The meta distribution of SINR in UAV-assisted cellular networks. *IEEE Trans. Commun.* **2023**, *71*, 1193–1206. [\[CrossRef\]](#)
4. Hayat, S.; Yanmaz, E.; Muzaffar, R. Survey on unmanned aerial vehicle networks for civil applications: A communications viewpoint. *IEEE Commun. Surv. Tutor.* **2016**, *18*, 2624–2661. [\[CrossRef\]](#)
5. Hua, B.; Ni, H.; Zhu, Q.; Wang, C.-X.; Zhou, T.; Mao, K.; Bao, J.; Zhang, X. Channel modeling for UAV-to-ground communications with posture variation and fuselage scattering effect. *IEEE Trans. Commun.* **2023**, *71*, 3103–3116. [\[CrossRef\]](#)
6. Mao, K.; Zhu, Q.; Song, M.; Li, H.; Ning, B.; Pedersen, G.F.; Fan, W. Machine-learning-based 3-D channel modeling for U2V mmWave communications. *IEEE Internet Things J.* **2022**, *9*, 17592–17607. [\[CrossRef\]](#)
7. da Silva, H.T.P.; de Alencar, M.S.; Assis, K.D.R. Path loss and delay spread characterization in a 26 GHz mmWave channel using the ray tracing method. In Proceedings of the IMOC'19, Aveiro, Portugal, 10–14 November 2019; pp. 1–3. [\[CrossRef\]](#)
8. Ravuri, V.; Subbarao, M.V.; Terlapu, S.K.; Ram, G.C. Path loss modeling and channel characterization at 28 GHz 5G micro-cell outdoor environment using 3D ray-tracing. In Proceedings of the ICAECT'22, Bhilai, India, 21–22 April 2022; pp. 1–7. [\[CrossRef\]](#)
9. Mani, F.; Vitucci, E.M.; Barbiroli, M.; Fuschini, F.; degli Esposti, V.; Gan, M.; Li, C.; Zhao, J.; Zhong, Z. 26GHz ray-tracing pathloss prediction in outdoor scenario in presence of vegetation. In Proceedings of the EuCAP'18, London, UK, 9–13 April 2018; pp. 1–5. [\[CrossRef\]](#)
10. Leonor, N.R.; Sánchez, M.G.; Fernandes, T.R.; Caldeirinha, R.F.S. A 2D ray-tracing based model for wave propagation through forests at micro-and millimeter wave frequencies. *IEEE Access* **2018**, *6*, 32097–32108. [\[CrossRef\]](#)
11. Wang, J.; Zhu, Q.; Lin, Z.; Wu, Q.; Huang, Y.; Cai, X.; Zhong, W.; Zhao, Y. Sparse bayesian learning-based 3D radio environment map construction—Sampling optimization, scenario-dependent dictionary construction and sparse recovery. *IEEE Trans. Cogn. Commun. Netw.* **2023**, *Accepted*. [\[CrossRef\]](#)
12. Mei, S.; Zhang, M.; Zhang, S.; Yu, C.; Luo, J.; Fu, Q.; Hu, S.; Liu, Y.; Wang, C.X. Characteristics analysis on NB-IoT channels in rural scenario for smart grid communications. In Proceedings of the ISAPE'21, Zhuhai, China, 1–4 December 2021; pp. 1–3. [\[CrossRef\]](#)
13. Suman, S.; Kumar, S.; De, S. Path loss model for UAV-assisted RFET. *IEEE Commun. Lett.* **2018**, *22*, 2048–2205. [\[CrossRef\]](#)
14. Pal, P.; Sharma, R.P.; Tripathi, S.; Kumar, C.; Ramesh, D. 2.4 GHz RF received signal strength based node separation in WSN monitoring infrastructure for millet and rice vegetation. *IEEE Sens. J.* **2021**, *21*, 18298. [\[CrossRef\]](#)
15. Phaiboon, S.; Phokharatkul, P. An empirical model for 433 MHz LoRa-WAN in ruby mango plantation. In Proceedings of the ICEAST'23, Vientiane, Laos, 20–23 March 2023; pp. 25–28. [\[CrossRef\]](#)
16. Vuran, M.C.; Lunar, M.M.; Nie, S.; Ge, Y.; Pitla, S.; Bai, G.; Koksals, C.E. Millimeter-wave agricultural channel measurements in corn and soybean fields at different growth stages. In Proceedings of the AP-S/URSI'22, Denver, CO, USA, 10–15 July 2022; pp. 1686–1687. [\[CrossRef\]](#)
17. Juan-Llácer, L.; Molina-García-Pardo, J.M.; Sibille, A.; Torrico, S.A.; Rubiola, L.M.; Martínez-Inglés, M.T.; Rodríguez, J.V.; Pascual-García, J. Path loss measurements and modelling in a citrus plantation in the 1800 MHz, 3.5 GHz and 28 GHz in LoS. In Proceedings of the EuCAP'22, Madrid, Spain, 27 March–1 April 2022; pp. 1–5. [\[CrossRef\]](#)
18. Nie, S.; Lunar, M.M.; Bai, G.; Ge, Y.; Pitla, S.; Koksals, C.E.; Vuran, M.C. mmWave on a farm: Channel modeling for wireless agricultural networks at broadband millimeter-wave frequency. In Proceedings of the SECON'22, Stockholm, Sweden, 1–3 June 2022; pp. 388–396. [\[CrossRef\]](#)
19. Liu, J.; Yu, J.; Niyato, D.; Zhang, R.; Gao, X.; An, J. Covert ambient backscatter communications with multi-antenna tag. *IEEE Trans. Wirel. Commun.* **2023**, *22*, 6199–6212. [\[CrossRef\]](#)
20. Saba, N.; Mela, L.; Sheikh, M.U.; Salo, J.; Ruttik, K.; Jäntti, R. Rural macrocell path loss measurements for 5G fixed wireless access at 26 GHz. In Proceedings of the 5GWF'21, Montreal, QC, Canada, 13–15 October 2021; pp. 328–333. [\[CrossRef\]](#)
21. HJawad, H.M.; Jawad, A.M.; Nordin, R.; Gharghan, S.K.; Abdullah, N.F.; Ismail, M.; Abu-AlShaeer, M.J. Accurate empirical path-loss model based on particle swarm optimization for wireless sensor networks in smart agriculture. *IEEE Sens. J.* **2020**, *20*, 552–561. [\[CrossRef\]](#)
22. Supramongkonset, J.; Duangsuwan, S.; Promwong, S. A WiFi link budget analysis of drone-based communication and IoT ground sensors. In Proceedings of the ICEAST'21, Pattaya, Thailand, 1–3 April 2021; pp. 234–237. [\[CrossRef\]](#)
23. Alnatoor, M.A.A.; Omari, M.; Kaddi, M. Modeling losses of mobile networks using artificial intelligence techniques. In Proceedings of the ICMIT'20, Adrar, Algeria, 18–19 February 2020; pp. 212–215. [\[CrossRef\]](#)
24. Moraitis, N.; Tsipi, L.; Vouyioukas, D.; Gkioni, A.; Louvros, S. Performance evaluation of machine learning methods for path loss prediction in rural environment at 3.7 GHz. *Wirel. Netw.* **2021**, *27*, 4169–4188. [\[CrossRef\]](#)
25. Pal, P.; Sharma, R.P.; Tripathi, S.; Kumar, C.; Ramesh, D. Machine learning regression for RF path loss estimation over grass vegetation in IoWSN monitoring infrastructure. *IEEE Trans. Ind. Inform.* **2022**, *10*, 6981–6990. [\[CrossRef\]](#)

26. Kayaalp, K.; Metlek, S.; Genç, A.; Dogan, H.; Basyigit, I.B. Breaking the uncertainty of path loss in coastal and vegetative environments with deep learning at 5g band. *SSRN Electron. J.* **2022**. [[CrossRef](#)]
27. Pan, J.; Ye, N.; Yu, H.; Hong, T.; Al-Rubaye, S.; Mumtaz, S.; Al-Dulaimi, A.; Chih-Lin, I. AI-driven blind signature classification for IoT connectivity: A deep learning approach. *IEEE Trans. Wirel. Commun.* **2022**, *8*, 6033–6047. [[CrossRef](#)]
28. Moraitis, N.; Tsipi, L.; Vouyioukas, D.; Gkioni, A.; Louvros, S. On the assessment of ensemble models for propagation loss forecasts in rural environments. *IEEE Wirel. Commun. Lett.* **2022**, *11*, 1097–1101. [[CrossRef](#)]
29. Duangsuwan, S.; Maw, M.M. Comparison of path loss prediction models for UAV and IoT air-to-ground communication system in rural precision farming environment. *J. Commun.* **2021**, *16*, 60–66. [[CrossRef](#)]
30. Rappaport, T.S. *Wireless Communications: Principles and Practice*; Prentice Hall PTR: Hoboken, NJ, USA, 2002.
31. Zhu, Q.; Wang, C.; Hua, B.; Mao, K.; Jiang, S. *3GPP TR 38.901 Channel Model*; Wiley Press: Hoboken, NJ, USA, 2021; pp. 1–35.
32. Maas, A.L.; Hannun, A.Y.; Ng, A.Y. Rectifier nonlinearities improve neural network acoustic models. In Proceedings of the ICML'13, Atlanta, GA, USA, 16–21 June 2013.
33. Mao, K.; Zhu, Q.; Qiu, Y.; Liu, X.; Song, M.; Fan, W.; Kokkeler, A.B.J.; Miao, Y. A UAV-aided real-time channel sounder for highly dynamic non-stationary A2G scenarios. *IEEE Trans. Instrum. Meas.* **2023**, *8*, 1–15. [[CrossRef](#)]

Disclaimer/Publisher's Note: The statements, opinions and data contained in all publications are solely those of the individual author(s) and contributor(s) and not of MDPI and/or the editor(s). MDPI and/or the editor(s) disclaim responsibility for any injury to people or property resulting from any ideas, methods, instructions or products referred to in the content.